Nanoscale

Accepted Manuscript

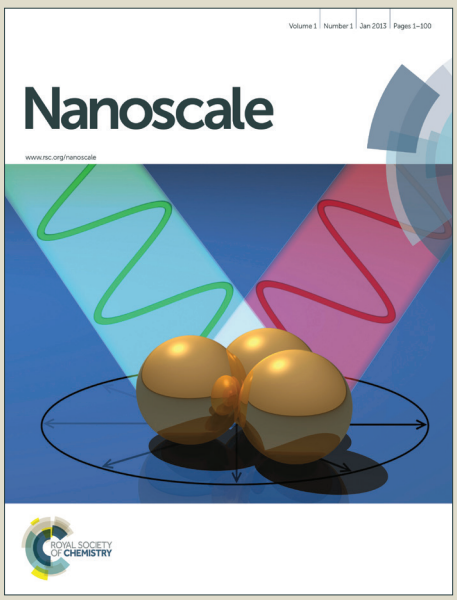

ROYAL SOCIETY OF CHEMISTRY

www.rsc.org/nanoscale

Nanoscale

RSCPublishing

COMMUNICATION

Correlated Structural-Optical Study of Single Nanocrystals in a Gap-bar Antenna: Effects of Plasmonics on Excitonic Recombination Pathways

Cite this: DOI: 10.1039/x0xx00000x

Received ooth January 2015,
Accepted ooth January 2015

DOI: 10.1039/x0xx00000x

www.rsc.org/

Feng Wang,[a] Niladri S. Karan,[a] Hue Minh Nguyen,[a] Yagnaseni Ghosh,[a,b] Chris J. Sheehan,[a] Jennifer A. Hollingsworth[a] and Han Htoon*[a]

We performed time–correlated single–photon counting experiments on individual silica coated CdSe/CdS core/thick-shell nanocrystal quantum dots (a.k.a., giant NQDs [g-NQDs]), placed on the plasmonic gap-bar antennas. Optical properties were directly correlated with the scanning electron microscopy (SEM) images of g-NQD-plamonic antenna coupled structures. The structures, in which the g-NQDs are located in the gap of the antenna, afford a coupling with up to 9.6 fold enhancement of radiative recombination rates. These coupled g-NQDs are also characterized by a strong enhancement of bi-exciton emission efficiency that increases with their radiative enhancement factor. By analysing these findings with a simple model, we show that the plasmonic field of the antenna does not alter the Auger recombination processes of the bi-exciton states. As a result, enhancements of the single and bi-exciton radiative recombination rates lead directly to bi-exciton emission enhancement. These findings suggest that a plasmonic field can be utilized effectively in achieving a strong bi-exciton emission that is needed for photon pair generation and plasmon-assisted lasing.

Plasmonic nano-antennas capable of providing a strong enhancement of light-matter interactions[1-3] have been explored extensively as a means for manipulating emission pattern,[4-6] polarization,[7] and excitonic recombination pathways of colloidal nanocrystal quantum dots (NQDs),[8-10] for a wide variety of technological applications including sensing,[11] light harvesting,[12] and solid state lighting.[13] Since this enhancement of light-matter interactions relies upon confinement of an electromagnetic field into a nanoscale region of antenna, an optimization of the NQD-antenna alignment is critical for the success of this approach. Intense research efforts in this area have resulted in several bottom-up self-assembly approaches[14, 15] as well as top-down electron beam lithography based approaches[9] capable of providing desired alignments. Even these approaches produce nanostructures exhibiting inhomogeneity in optical behaviours resulting from slight variations in alignments and organization. Therefore, characterization of these structures demands an ability to perform nanometer resolution imaging and advanced optical spectroscopy studies on the same nanostructure.

Recently, single–nanostructure spectroscopy was performed together with scanning electron microscopy (SEM) or atomic force microscopy (AFM) to establish a direct correlation between structures and plasmonic effects.[16, 17] These studies proved to be very powerful in understanding plasmonic response of three dimensional plasmonic nanoclusters.[18, 19] They also revealed many insights into plasmonic antenna-emitter coupled systems including multipolar radiation of quantum emitters,[6] dependence of blinking suppression upon NQD-emitter separation,[17, 20] differences between excitation and emission enhancement processes,[9, 21] and unidirectional emission of NQD-antenna coupled systems.[4] However, this type of experiment has not been applied so far in an investigation of plasmonic effects on recombination of multi-excitonic states that are important for technological applications such as entangled photon generation,[22-26] light amplification,[27] and plasmon-assisted lasing.[28, 29]

Unlike single excitons, multi-exciton states of NQDs can recombine non-radiatively via Auger recombination processes that occurs through carrier-carrier Coulomb interaction.[30] Plasmonic nano-antenna can provide additional contribution to the Auger matrix elements via charge-image interaction. On the other hand Ohmic losses and enhanced radiative decay can suppress the latter process. Interplay of these effects is not fully understood. Furthermore, it is also speculated that the plasmonic field of the antenna can break the symmetry of multi-exciton states and open new radiative recombination pathways.[31] Recent optical spectroscopy studies in this area have revealed that emission of multi-exciton states is strongly enhanced relative to that of single excitons.[31-34] However, while some studies suggest that the relative enhancement of multi-exciton emission efficiency results mainly from metal-induced PL quenching of single exciton emission efficiency,[34, 35] the findings of other studies can be explained only if there are some changes in the nature of multi-exciton recombination processes.[31, 33, 36] A unified understanding of this topic could introduce a new plasmonic approach for control of multi-exciton recombination processes.

Toward realizing such understanding, we performed a correlated SEM-optical spectroscopy study on individual NQDs

deterministically placed inside the gap-bar antenna. In this experiment, we utilized a new class of non-blinking NQDs that are often referred to as giant-NQDs (g-NQDs) in which a 4-nm CdSe core is over-coated with a 16-monolayer-thick CdS shell.[37, 38] Our previous studies, in which g-NQDs were placed directly upon a rough silver surface, revealed clear evidence of the strong enhancement of bi-exciton emission relative to that of a single exciton.[32] This enhancement, however, is accompanied by 90% quenching of the PL emission suggesting that the relative enhancement resulted more from the drastic reduction of single exciton quantum yield than an actual increase of the bi-exciton emission efficiency. We have attributed this PL quenching to non-radiative decay of excitons via intra-gap recombination centres formed at the g-NQD–silver interface or direct charge tunnelling into the proximal silver.[32] To investigate plasmonic enhancement effects without the collusion of these unwanted PL quenching channels, we over-coated our g-NQDs with a 10–nm–thick silica shell (see Supp. Info. S1).[39] This silica shell also protects the PL of the g-NQDs from quenching through a Förster energy transfer to the metal.

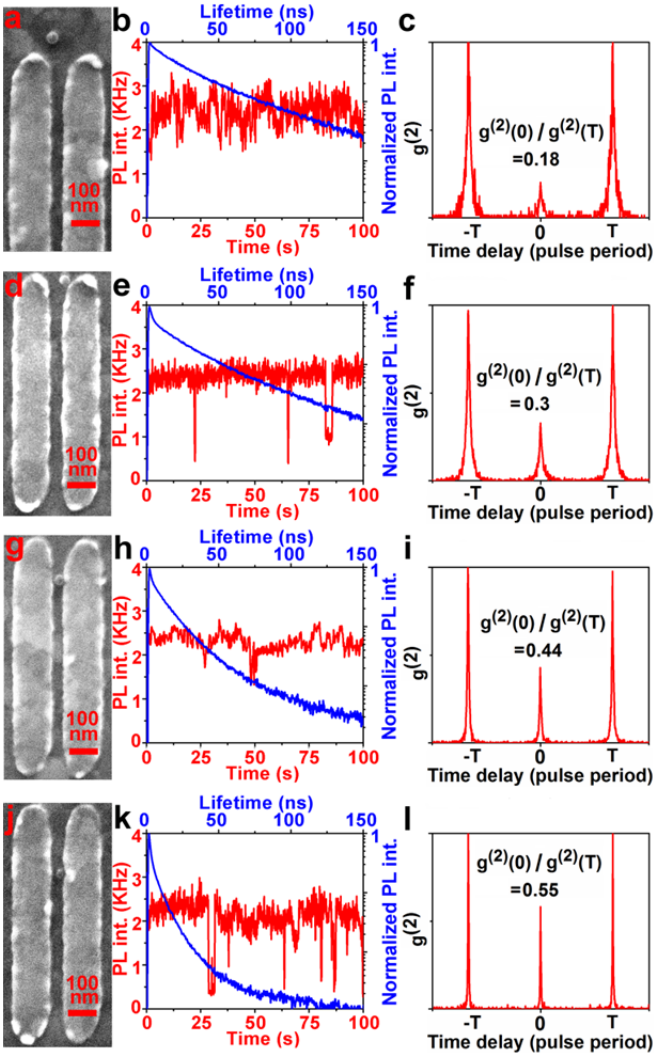

Fig. 1 a), d), g) and j) are the SEM images of four representative g-NQD–antenna coupled structures with different degrees of alignment; b), e), h) and k) are the measured PL time traces (red) and lifetime decay curves (blue); c), f), i), and l) are the measured g(2) traces corresponding to each SEM picture.

We placed these g-NQDs into the gap of the antenna structures by using a two-step e-beam lithography process[9] described in Supp. Info. S2. As displayed in Fig. 1a the antennas are made of two gold bars with length, width, thickness, and gap sizes of 900, 140, 45, and 55 nm, respectively. The measured antenna scattering spectrum (see Supp. Info. S3) indicates that the resonant wavelength of the antenna agrees well with the emission wavelength of the g-NQDs. A time–tagged, time–correlated single photon counting experiment was then performed to acquire PL time traces, decay curves, and second order photon correlation functions of isolated individual emission spots. The g-NQDs are excited by a picosecond laser at 405 nm. The laser repetition rate is set to 1 MHz to allow for a complete relaxation of exciton population. SEM imaging was performed after the completion of all the optical studies to avoid altercation of optical properties resulting from e-beam induced charging. Reference markers fabricated together with the gap-bar antennas were used to locate the exact g-NQD–antenna coupled structures investigated in the optical study.

Figure 1 displays SEM images, PL time traces, decay curves and second order photon correlation functions of four representative g-NQD–antenna coupled structures with different degrees of alignments. While g-NQDs of Fig. 1a and 1d are located 100 and 20 nm away from the narrowest gap of the antenna, the g-NQDs of Fig. 1g and 1j are located fully inside the gap of the antenna. PL time traces (red traces of Fig. 1b, 1e, 1h, 1k) show nearly blinking free PL emission at 2–3 kHz count rate for these representative g-NQDs. All of the 19 single g-NQD–antenna coupled structures investigated in this study exhibit similar emission behaviour with count rates distributed in the 1.5 – 2.5 kHz range (Fig. 2a red bars). Another 19 silica–coated g-NQDs spread on glass, which are investigated as a reference, show nearly identical suppressed blinking behaviour (see Supp. Info. S4) with a PL count rate distributed in a slightly higher range of 2–3 KHz (Fig. 2a blue bars). These data indicate that metal-induced PL quenching is small in this experiment (see Supp. Info. S5 for details).

Conversely, PL decay curves (blue traces of Fig. 1b, 1e, 1h, 1k) show clear enhancement of the PL decay rate with an increase of g-NQD–antenna coupling. The fit–to–decay curves yield an average decay constant of 50.0, 30.1, 14.9, and 7.7 ns, respectively. The decay constants of all the 19 g-NQDs coupled to antennas are distributed in the 5–45 ns range (Fig. 2b red bars) whereas the decay constants of the reference g-NQD are distributed in the 40–80 ns range with an average value of 63.3 ns (Fig. 2b blue bars). With respect to this average lifetime, the decay rates of the QDs in Fig. 1a, 1d, 1g and 1j are enhanced by the factors of 1.25, 2.1, 4.2, and 8.2, respectively. The decay rate enhancement factors of other QDs are distributed in the range of 1.4–9.6 (Fig. 2c red bars). We also observed that g-NQDs that are coupled to the antenna also emit PL strongly polarized in the direction perpendicular to the length of the bar, as shown in Fig. 2e. The degree of polarization (defined as $[I_{\perp} - I_{\parallel}]/[I_{\perp} + I_{\parallel}]$) of 19 single g-NQD–antenna structures decrease with the increase of the PL lifetime, as shown in Fig. 2f.

Second order photon correlation functions (Fig. 1c, 1f, 1i, 1l) show an increase in the center to side peak area ratio (R=g$^{(2)}$(0)/g$^{(2)}$(T)) from 0.18 to 0.55 in correlation with the enhancement of the decay rates. R values of other g-NQDs on plasmonic antennas (R_p) are distributed in the range of 0.3–0.7 (Fig. 2d red bars) and also show a rapid increase with the decrease of lifetime (Fig. 2g red data points). In contrast, the R values of the reference g-NQDs (R_{ref}) lie below 0.25 with an average of 0.15 (Fig. 2d blue bars) and exhibit only a weak dependence on lifetime (Fig. 2g blue data points). For a single QD excited at low pump fluence where average exciton occupancy is <0.2, R can also be defined mainly as the ratio between quantum yield of single and bi-exciton

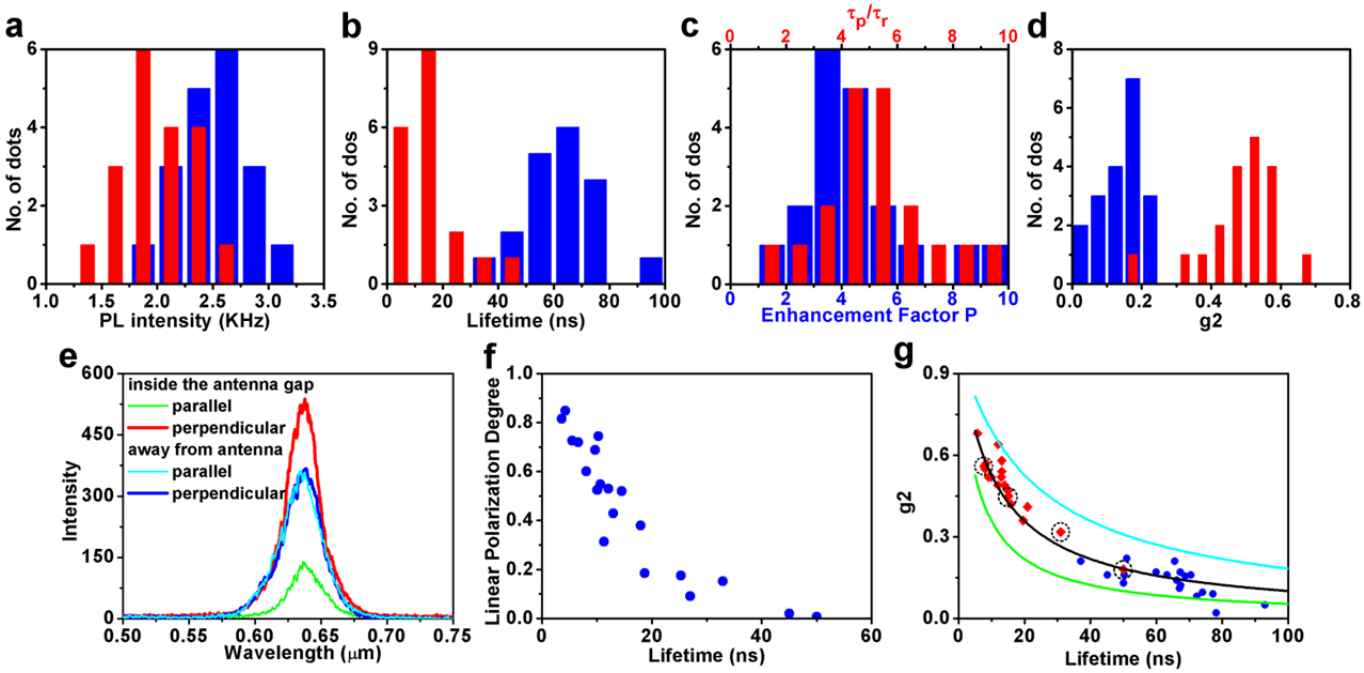

Fig. 2 a) Histograms of PL intensities of single g-NQDs placed on glass (blue) and on gap bar antennas (red).; b) Histograms of lifetimes of single g-NQDs when placed on glass (blue) and on gap bar antennas (red); c) Histograms show the distribution of decay rate enhancement (red) and emission enhancement (blue) for single g-NQDs placed on the nano-antennas; d) Histograms show the distribution of $g^{(2)}$ for single g-NQDs on glass (blue) and on nano-antennas (red); e) Measured emission spectra of g-NQD of Fig.1a with polarization parallel (cyan) and perpendicular (blue) to the antenna's long axis and measured emission spectra of g-NQDs of Fig. 1g with polarization parallel (green) and perpendicular (red) to the antenna's long axis; f) Measured linear polarization degree of 19 g-NQDs–antennas coupled structures as a function of PL lifetime; g) Measured $g^{(2)}$ as the function of measured lifetime for reference g-NQDs (blue scatters) and g-NQDs-antennas coupled structures (red scatters). Calculated $g^{(2)}$ as the function of lifetime for different Auger recombination parameters (q) with q=0.5 (cyan), q=1 (black) and q=2 (green). Black dotted circles mark the data points for the four representative g-NQDs shown in Fig. 1.

states (R= Q_{2X}/Q_{1X}) (see Supp. Info. S6 for details).[36, 40] These results indicate an enhancement of bi-exciton emission relative to that of a single exciton.

This enhancement of R_p could result from a change in the competition between the radiative and non-radiative recombination processes of bi-excitons or simply from creating more excitons due to plasmonic enhancement of the 405 nm excitation laser field.[31] To distinguish between these two contributions, we analysed the pump dependent PL saturation behaviours of one uncoupled g-NQD and one coupled g-NQD-antenna structure as in Fig. 1a and Fig. 1g. Consistent with a low R_{ref} value of 0.18, the uncoupled g-NQD-antenna exhibits a strong PL saturation (Fig. 3a).[36] While the PL of the coupled g-NQD-antenna increases with pump power in a way very similar to the uncoupled QD-antenna at low pump power range, the PL shows a much weaker saturation at higher pump powers indicating a higher Q_{2X} (Fig. 3b).[36] For further quantitative analysis, we described PL intensity in terms of average exciton population $\langle N\rangle$ as

$$\mathrm{I(w)} = \mathrm{C}\sum_{\mathrm{N}=1}^{\infty}\mathrm{P}\left(\mathrm{N},\langle\mathrm{N}\rangle\right)\sum_{\mathrm{m}=1}^{\mathrm{N}}Q_{mX} \qquad (1)$$

where

$$\mathrm{P}\left(\mathrm{N},\langle\mathrm{N}\rangle\right) = \langle\mathrm{N}\rangle^{N}\, e^{-\langle\mathrm{N}\rangle} / N! \qquad (2)$$

is the Poisson distribution defining the probability of exciting N^{th} multi-exciton states when a g-NQD is populated on average with $\langle\mathrm{N}\rangle$ excitons per excitation pulse, C is a constant mainly representing the photon collection efficiency of the measurement system, and Q_{mX} is the quantum yield of m-exciton state respectively.[36] $\langle N\rangle$ is related to laser power (w) as

$$\langle N\rangle = \mathrm{Aw}, \text{ with } \mathrm{A} = \sigma/\mathrm{RDE_{ph}} \qquad (3)$$

where σ, R, D and E_{ph} representing g-NQD absorption cross-setion, laser repetition rate, laser spot area and photon energy respectively. Using statistical scaling law, we also expressed Q_{mX} in terms of Q_{2X} as (see Supp. Info S7)

$$Q_{mX} = 1/(1+(m-1)(1-Q_{2X})/Q_{2X})\,. \qquad (4)$$

Combining equation 1-4 yields the model that describe I(w) in term of Q_{2X} and the proportionality constant A that provide a direct measure of σ. Fitting PL saturation data of Fig. 3 to this model produced Q_{2X} of 0.17 and 0.43 for the two dots of Fig. 1a and Fig. 1g respectively, which is in excellent agreement with the R_{ref} = 0.18 and R_p= 0.44 values attained from the $g^{(2)}$ traces. More important, the fit produced two very similar values (9.0 and 8.5) for constant A, suggesting that σ of the g-NQD on the antenna is essentially the same as that of the uncoupled QD. This experiment, therefore, leads us to the conclusion that plasmon induced changes in recombination dynamic of bi-excitons is responsible for the enhancement of R_P.

To understand this enhancement and its rapid decrease with the increase of lifetime, we analysed how a plasmonic field could affect quantum yields of single and bi-exciton states through modification to radiative and Auger decay rates. When a g-NQD with unity Q_{1X} and radiative decay rate of k_r^X is coupled to a plasmonic antenna, total decay rate k_{TP}^X is enhanced due to enhancement of radiative rate

by a factor (p) and non-radiative decay of exciton via energy transfer to the metal (k_{nr}^{X}), i.e.,

$$k_{TP}^{X} = pk_{r}^{X} + k_{nr}^{X}. \quad (5)$$

Then Q_{1X} will be reduced from unity to

$$Q_{1XP} = 1/(1 + k_{nr}^{X} / pk_{r}^{X}). \quad (6)$$

The enhancement factor p can be calculated from Eqn (5) and (6) as

$$p = (I_P / I_R)(\tau_R / \tau_P). \quad (7)$$

where, under low pump power, $\tau_{R(P)} = 1/k_{r(TP)}^{X}$ and $I_P \propto Q_{1XP}$ ($I_R \propto Q_{1X}$) represent the PL intensity of the g-NQD on antenna (the referenced g-NQD) respectively. By taking the average PL count rate and lifetime of the reference g-NQDs as I_R and τ_R , we calculate the p values for each of g-NQD on antenna from their experimentally measured intensity and lifetimes. Because the PL intensity of g-NQDs on antenna is reduced only slightly from the reference g-NQDs (Fig. 2a), for most of the g-NQDs the p values are essentially the same as the ratio of the lifetimes. The distribution of the p values is plotted together with the total lifetime enhancement factor in Fig. 2c.

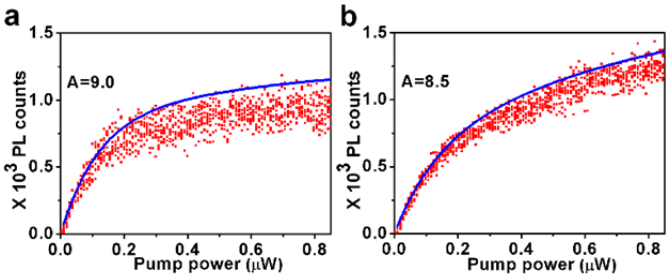

Fig. 3 a) and b) measured (red) and fitted (blue) PL saturation behavior of single g-NQDs as the function of laser pump power. While a) corresponds to the QD/antenna alignment shown in Fig.1a, b) corresponds to the alignment shown in Fig. 1g. The fit to the measured saturation was performed for the data points in the top 5% of intensity since those data point are most likely the emissions from neutral excitons having near unity quantum yield.

To analyse the effect of plasmon on bi-exciton recombination, we firstly invoke the fact that radiative and Förster energy transfer rates of bi-excitons scale up from those of single exciton state according to the increase in number of available recombination channels (i.e. $k_{r/nr}^{2X} = 4k_{r/nr}^{X}$). We then express the total bi-excitons decay rate (k_{T}^{2X}) and R_{ref} for referenced g-NQDs as

$$k_{T}^{2X} = 4k_{r}^{X} + k_{A}^{2X}\ ;\ R_{ref} = Q_{2X} = \frac{1}{1 + k_{A}^{2X} / 4k_{r}^{X}} \quad (8)$$

where k_{A}^{2X} is the Auger recombination rate of the bi-exciton. Next we assume that coupling of a g-NQD to an antenna enhances the radiative rate of the bi-exciton by the same factor as that of the single exciton (i.e. $k_{rP}^{2X} = 4pk_{r}^{X}$) and Auger recombination rates of bi-exitons is modified by a factor q, we express total decay rate of a bi-exciton states and Q_{2X} (k_{TP}^{2X} , Q_{2X}^{P}) as

$$k_{TP}^{2X} = 4pk_{r}^{X} + 4k_{nr}^{X} + qk_{A}^{2X};\ \ Q_{2X}^{P} = \frac{1}{1 + k_{nr}^{X} / pk_{r}^{X} + q\,k_{A}^{2X} / 4pk_{r}^{X}} \quad (9)$$

By combining Eqs. 5-9, we express R_P as a function of R_{ref} and τ_R / τ_P as

$$R_P = \frac{\tau_R / \tau_P}{\tau_R / \tau_P + q(1 - R_{ref}) / R_{ref}} \quad (10)$$

We calculate R_P as the function of τ_P for different q values of 1, 0.5 and 2 using averaged lifetime and R values of the referenced g-NQDs (63.3 ns and 0.15) as R_{ref} and τ_R , respectively, in Eq. (10). The plot for q=1 (black curve of Fig. 2g) represents the case in which plasmonic field has no effect on Auger recombination rate. Whereas the q=0.5 (2.0) plots [blue (green) curve of Fig. 2g] is for the condition in which the plasmonic field suppresses (enhances) the Auger rate by a factor of 2. The curves show that our simple model can explain the decrease of the R values as a direct consequence of reduction in lifetime enhancement (τ_R / τ_P). More important, based on the appearance of all the data points (red squares of Fig. 2g) in the region between the q=1 and q=0.5 curve, we can conclude that the plasmonic field most likely has no effect on Auger recombination.

Finally for further validation, we compared our findings with the results of our finite integration numerical simulations[41] using CST Microwave studio (see Supp. Info. S8). We first calculated the enhancement of the laser excitation field as the ratio of energy flux transmitting through the volume of g-NQDs with and without the plasmonic antennas. The calculation for various configurations yields enhancement factor values around 1.05, indicating a negligible local enhancement of excitation field (Fig. 4a). This result, therefore, provides further confirmation that the enhanced decay rate is not due to the enhanced excitation but due to the enhanced coupling between QD emission and nano-antennas. Next we placed a linear dipole representing a g-NQD on the plane of the antenna (x-y plane) and investigated near-field distribution of dipoles, enhancement factors and degree of linear polarization. The orientation of dipole is set to be 45° off the long axis of the gap bar (x-axis) so that both x and y polarized emission could be calculated. Near-field distributions of three g-NQDs with QD-antenna-separations closely representing those shown in Fig. 1a, 1d, and 1j (i.e., 100, 20 nm away from one end of the gap-bar and at the centre of the gap-bar, respectively) are displayed in Fig. 4b–4d. The data show that while the near-field of the g-NQD in the centre of the gap bar (Fig. 4d) is coupled to the plasmonic modes of the antenna, the coupling decreases significantly for the g-NQDs 20 and 100 nm away from the end (Fig. 4c and Fig. 4b).

To determine emission enhancement and polarization, we integrated the square of electric fields (E^2) determined at 25 far-field locations that are distributed homogeneously over the cone defined by the numerical aperture of our experiment. Emission enhancement factor at a wavelength is then calculated as a ratio between E^2 of the dipole-antenna coupled structure and that of an isolated dipole (E_0^2). For a continuously excited dipole considered in this simulation, this emission enhancement factor should be identical to the enhancement of the PL decay rate.[42, 43] The calculated intensity enhancement spectra (E^2/E_0^2) (Fig. 4e) show a peak at 640nm in perfect match with the emission spectra of the g-NQDs. For the g-NQD in the middle of the gap (blue curve), the spectrum gives the peak enhancement factor of 10.8. The weighted average of the emission enhancement over the whole emission spectrum of our g-NQDs is 9.8, which actually is in good agreement with the measured highest emission enhancement of 9.6. The simulation further shows that this

enhancement factor decreases to 3.4 for the dipole at 20 nm QD-antenna separation and to1.0 at 100 nm.

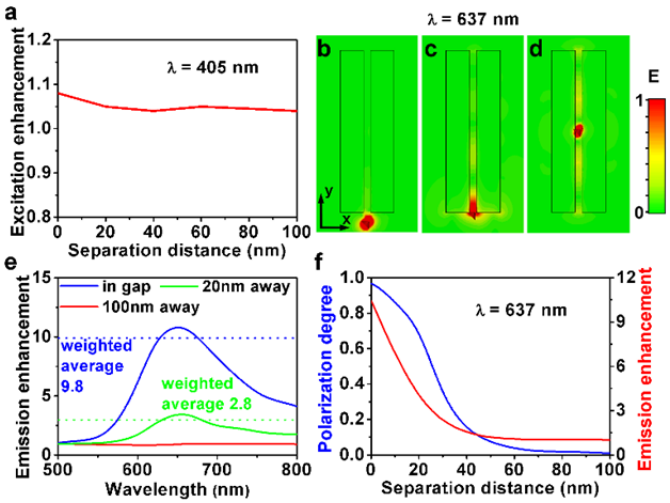

Fig. 4 a) Enhancement of 405 nm excitation as the function of separation distance between g-NQDs and antenna gap; Near field distributions show the coupling strengths for g-NQDs placed 100 nm away from the gap b); 20 nm away from the gap c) and inside the gap d); e) Emission enhancement spectra of the silica coated g-NQDs placed along the long axis of the gap. Blue curve: totally positioned inside gap; Green curve: 20 nm away from the gap; Red curve: 100 nm away from the gap; f) Linear polarization degree of emission (blue) and enhancement of emission (red) as the function of separation distance between g-NQDs and antenna gap.

The plot of enhancement factor vs QD–antenna separation clearly shows that the enhancement actually has decreased to unity for separations larger than 60 nm (Fig. 4f, red curve). In addition to the QD–antenna separation, other factors such as fluctuations in width of the gap as well as orientation of the g-NQD dipole with respect to the antenna could lead to decrease of the enhancement factors from the maximum. Our calculation also shows that while the electric field along the x-axis is strongly enhanced, the field along y axis experiences a slight suppression. This results in an emission strongly polarized in the x direction for the g-NQDs coupled to the antennas (Fig. 4f blue curve), as observed experimentally.

Conclusions

In summary, our correlated structural-optical study of g-NQD/gap-bar antenna coupled structure revealed that the plasmonic field of the antenna can not only enhance the radiative decay rate of single exciton states by a factor as high as 9, it can also boost the relative emission efficiency of bi-exciton (R values) from <0.2 to those approaching unity (~0.7). Because the PL intensity of our g-NQDs on gap bars shows no quenching relative to that of the reference dots, we can state that the enhancement of R results not from the decrease of Q_{1X} but from a true increase of the Q_{2X}. A careful analysis of these results using a simple model further leads to an important conclusion that the plasmonic field of the antenna most likely has no effect on Auger recombination of bi-excitons. Enhancement of radiative decay rates, therefore, directly translated to the enhancement of Q_{2X}. These findings together point to the fact that g-NQD–antenna coupled structures could be highly beneficial for applications requiring efficient emission of bi-exciton such as entangled photon generation[25, 26] and plasmon assisted lasing.[24, 28]

Acknowledgements

This work was supported by a Single Investigator Small Group Research Grant (2009LANL1096), Division of Materials Science and Engineering (MSE), Office of Basic Energy Sciences (OBES), Office of Science (OS), U.S. Department of Energy (DOE) and conducted at the Center for Integrated Nanotechnologies (CINT), a U.S. DOE, OBES Nanoscale Science Research Center and User Facility. We thank Andrei Piryatinski of LANL, Theoretical Division for a discussion.

Notes and references

[a]Center for Integrated Nanotechnologies, Materials Physics & Applications Division, Los Alamos National Laboratory, Los Alamos, New Mexico 87545. E-mail: htoon@lanl.gov
[b]Current Address: Pacific Light Technologies, 2828 SW Corbett Avenue, Suite 111, Portland, OR 97201.
†Electronic Supplementary Information (ESI) available. See DOI: 10.1039/c000000x/

1 J. A. Schuller, E. S. Barnard, W. Cai, Y. C. Jun, J. S. White and M. L. Brongersma, *Nat. Mater.*, 2010, **9**, 193-204.
2 P. Mühlschlegel, H.-J. Eisler, O. J. F. Martin, B. Hecht and D. W. Pohl, *Science*, 2005, **308**, 1607-1609.
3 M. S. Tame, K. R. McEnery, S. K. Ozdemir, J. Lee, S. A. Maier and M. S. Kim, *Nat Phys*, 2013, **9**, 329-340.
4 A. G. Curto, G. Volpe, T. H. Taminiau, M. P. Kreuzer, R. Quidant and N. F. van Hulst, *Science*, 2010, **329**, 930-933.
5 N. P. de Leon, B. J. Shields, L. Y. Chun, D. E. Englund, A. V. Akimov, M. D. Lukin and H. Park, *Phys. Rev. Lett.*, 2012, **108**, 226803.
6 A. G. Curto, T. H. Taminiau, G. Volpe, M. P. Kreuzer, R. Quidant and N. F. van Hulst, *Nat Commun.*, 2013, **4**, 1750.
7 Q. Zhu, S. Zheng, S. Lin, T.-R. Liu and C. Jin, *Nanoscale*, 2014, **6**, 7237-7242.
8 T. V. Teperik and A. Degiron, *Phys. Rev. Lett.*, 2012, **108**, 147401.
9 E. B. Ureña, M. P. Kreuzer, S. Itzhakov, H. Rigneault, R. Quidant, D. Oron and J. Wenger, *Adv. Mater.*, 2012, **24**, OP314-OP320.
10 J. S. Biteen, D. Pacifici, N. S. Lewis and H. A. Atwater, *Nano Lett.*, 2005, **5**, 1768-1773.
11 S. L. Diedenhofen, D. Kufer, T. Lasanta and G. Konstantatos, *Light Sci. Appl.*, 2015, **4**, e234.
12 S. Jin, E. DeMarco, M. J. Pellin, O. K. Farha, G. P. Wiederrecht and J. T. Hupp, *J. Phys.Chem. Lett.*, 2013, **4**, 3527-3533.
13 H. A. Atwater, *Scientific American*, 2007, **296**, 56-62.
14 S. H. Ko, K. Du and J. A. Liddle, *Angew. Chem. Int. Ed.*, 2013, **52**, 1193-1197.
15 A. Samanta, Y. Zhou, S. Zou, H. Yan and Y. Liu, *Nano Lett.*, 2014, **14**, 5052-5057.
16 C. Belacel, B. Habert, F. Bigourdan, F. Marquier, J. P. Hugonin, S. Michaelis de Vasconcellos, X. Lafosse, L. Coolen, C. Schwob, C. Javaux, B. Dubertret, J. J. Greffet, P. Senellart and A. Maitre, *Nano Lett.*, 2013, **13**, 1516-1521.
17 D. Ratchford, F. Shafiei, S. Kim, S. K. Gray and X. Li, *Nano Lett.*, 2011, **11**, 1049-1054.
18 M. Creasey, J.-H. Lee, Z. Wang, G. J. Salamo and X. Li, *Nano Lett.*, 2012, **12**, 5169-5174.

19 A. S. Urban, X. Shen, Y. Wang, N. Large, H. Wang, M. W. Knight, P. Nordlander, H. Chen and N. J. Halas, *Nano Lett.*, 2013, **13**, 4399-4403.
20 Q. Li, H. Wei and H. Xu, *Nano Lett.*, 2014, **14**, 3358-3363.
21 K. Munechika, Y. Chen, A. F. Tillack, A. P. Kulkarni, I. J.-L. Plante, A. M. Munro and D. S. Ginger, *Nano Lett.*, 2010, **10**, 2598-2603.
22 D. E. Chang, A. S. Sørensen, E. A. Demler and M. D. Lukin, *Nat. Phys.*, 2007, **3**, 807-812.
23 R. W. Heeres, L. P. Kouwenhoven and V. Zwiller, *Nat Nano*, 2013, **8**, 719-722.
24 O. Astafiev, K. Inomata, A. Niskanen, T. Yamamoto, Y. A. Pashkin, Y. Nakamura and J. Tsai, *Nature*, 2007, **449**, 588-590.
25 A. Gonzalez-Tudela, D. Martin-Cano, E. Moreno, L. Martin-Moreno, C. Tejedor and F. J. Garcia-Vidal, *Phys. Rev. Lett.*, 2011, **106**, 020501.
26 M. T. Cheng, X. S. Ma, Y. Q. Luo, P. Z. Wang and G. X. Zhao, *Appl. Phys. Lett.*, 2011, **99**, 223509.
27 D. J. Bergman and M. I. Stockman, *Phys. Rev. Lett.*, 2003, **90**, 027402.
28 M. Nomura, N. Kumagai, S. Iwamoto, Y. Ota and Y. Arakawa, *Nat. Phys.*, 2010, **6**, 279-283.
29 Y.-J. Lu, J. Kim, H.-Y. Chen, C. Wu, N. Dabidian, C. E. Sanders, C.-Y. Wang, M.-Y. Lu, B.-H. Li, X. Qiu, W.-H. Chang, L.-J. Chen, G. Shvets, C.-K. Shih and S. Gwo, *Science*, 2012, **337**, 450-453.
30 V. Klimov, A. Mikhailovsky, D. McBranch, C. Leatherdale and M. Bawendi, *Science*, 2000, **287**, 1011-1013.
31 Y.-S. Park, Y. Ghosh, P. Xu, N. H. Mack, H.-L. Wang, J. A. Hollingsworth and H. Htoon, *J. Phys. Chem. Lett.*, 2013, **4**, 1465-1470.
32 Y.-S. Park, Y. Ghosh, Y. Chen, A. Piryatinski, P. Xu, N. H. Mack, H.-L. Wang, V. I. Klimov, J. A. Hollingsworth and H. Htoon, *Phys. Rev. Lett.*, 2013, **110**, 117401.
33 S. J. LeBlanc, M. R. McClanahan, M. Jones and P. J. Moyer, *Nano Lett.*, 2013, **13**, 1662-1669.
34 Y. Gao, O. Roslyak, E. Dervishi, N. S. Karan, Y. Ghosh, C. J. Sheehan, F. Wang, G. Gupta, A. Mohite and A. M. Dattelbaum, *Adv. Opt. Mater.*, 2014.
35 H.-W. Cheng, C.-T. Yuan, J.-S. Wang, T.-N. Lin, J.-L. Shen, Y.-J. Hung, J. Tang and F.-G. Tseng, *J. Phys. Chem. C*, 2014, **118**, 18126-18132.
36 Y. S. Park, A. V. Malko, J. Vela, Y. Chen, Y. Ghosh, F. García-Santamaría, J. A. Hollingsworth, V. I. Klimov and H. Htoon, *Phys. Rev. Lett.*, 2011, **106**, 187401.
37 Y. Ghosh, B. D. Mangum, J. L. Casson, D. J. Williams, H. Htoon and J. A. Hollingsworth, *J. Am. Chem. Soc.*, 2012, **134**, 9634-9643.
38 Y. Chen, J. Vela, H. Htoon, J. L. Casson, D. J. Werder, D. A. Bussian, V. I. Klimov and J. A. Hollingsworth, *J. Am. Chem. Soc.*, 2008, **130**, 5026-5027.
39 D. K. Yi, S. T. Selvan, S. S. Lee, G. C. Papaefthymiou, D. Kundaliya and J. Y. Ying, *J. Am. Chem. Soc.*, 2005, **127**, 4990-4991.
40 G. Nair, J. Zhao and M. G. Bawendi, *Nano Lett.*, 2011, **11**, 1136-1140.
41 T. Weiland, *Electron. and Commun. AEUE*, 1977, **31**, 116.
42 T. H. Taminiau, F. D. Stefani and N. F. van Hulst, *Opt. Express*, 2008, **16**, 10858-10866.
43 P. Anger, P. Bharadwaj and L. Novotny, *Phys. Rev. Lett.*, 2006, **96**, 113002.

